



## Article

# Desert Locust (*Schistocerca gregaria*) Invasion Risk and Vegetation Damage in a Key Upsurge Area

Raphael Mongare <sup>1,2</sup> , Elfatih M. Abdel-Rahman <sup>1</sup> , Bester Tawona Mudereri <sup>1,\*</sup> , Emily Kimathi <sup>1</sup>, Simon Onywere <sup>2</sup> and Henri E. Z. Tonnang <sup>1</sup>

<sup>1</sup> International Centre of Insect Physiology and Ecology (icipe), P.O. Box 30772, Nairobi 00100, Kenya

<sup>2</sup> Department of Spatial and Environmental Planning, School of Architecture and Built Environment, Kenyatta University, P.O. Box 43844, Nairobi 00100, Kenya

\* Correspondence: bmudereri@icipe.org

**Abstract:** In the recent past, the Horn of Africa witnessed an upsurge in the desert locust (*Schistocerca gregaria*) invasion. This has raised major concerns over the massive food insecurity, socioeconomic impacts, and livelihood losses caused by these recurring invasions. This study determined the potential vegetation damage due to desert locusts (DLs) and predicted the suitable habitat at high risk of invasion by the DLs using current and future climate change scenarios in Kenya. The normalized difference vegetation index (NDVI) for the period 2018–2020 was computed using multi-date Sentinel-2 imagery in the Google Earth Engine platform. This was performed to assess the vegetation changes that occurred between May and July of the year 2020 when northern Kenya was the hotspot of the DL upsurge. The maximum entropy (MaxEnt) algorithm was used together with 646 DL occurrence records and six bioclimatic variables to predict DL habitat suitability. The current (2020) and two future climatic scenarios for the shared socioeconomic pathways SSP2-4.5 and SSP5-8.5 from the model for interdisciplinary research on climate (MIROC6) were utilized to predict the future potential distribution of DLs for the year 2030 (average for 2021–2040). Using Turkana County as a case, the NDVI analysis indicated the highest vegetation damage between May and July 2020. The MaxEnt model produced an area under the curve (AUC) value of 0.87 and a true skill statistic (TSS) of 0.61, while temperature seasonality (Bio4), mean diurnal range (Bio2), and precipitation of the warmest quarter (Bio18) were the most important bioclimatic variables in predicting the DL invasion suitability. Further analysis demonstrated that currently 27% of the total area in Turkana County is highly suitable for DL invasion, and the habitat coverage is predicted to potentially decrease to 20% in the future using the worst-case climate change scenario (SSP5-8.5). These results have demonstrated the potential of remotely sensed data to pinpoint the magnitude and location of vegetation damage caused by the DLs and the potential future risk of invasion in the region due to the available favorable vegetational and climatic conditions. This study provides a scalable approach as well as baseline information useful for surveillance, development of control programs, and monitoring of DL invasions at local and regional scales.

**Keywords:** food security; insect pest upsurge; Kenya; MaxEnt; Sentinel-2; species distribution model; vegetation index



**Citation:** Mongare, R.; Abdel-Rahman, E.M.; Mudereri, B.T.; Kimathi, E.; Onywere, S.; Tonnang, H.E.Z. Desert Locust (*Schistocerca gregaria*) Invasion Risk and Vegetation Damage in a Key Upsurge Area. *Earth* **2023**, *4*, 187–208. <https://doi.org/10.3390/earth4020010>

Received: 5 February 2023

Revised: 15 March 2023

Accepted: 21 March 2023

Published: 28 March 2023



**Copyright:** © 2023 by the authors. Licensee MDPI, Basel, Switzerland. This article is an open access article distributed under the terms and conditions of the Creative Commons Attribution (CC BY) license (<https://creativecommons.org/licenses/by/4.0/>).

## 1. Introduction

Desert locusts (DLs), *Schistocerca gregaria*, are migratory pests that are part of a group of short-horned grasshoppers belonging to the *Acrididae* family [1]. They are a major threat to agriculture, forestry, and animal husbandry, leading to a vulnerability in the food and nutrition security systems and socioeconomic networks [2,3]. Particularly, the damage caused by DLs on farm- and pastureland is a threat to the food and nutrition security of over 60 countries in Africa, the Middle East, and Southwest Asia regions that account for approximately 10% of the world's human population [4,5]. Additionally, vegetation

loss due to DL invasions in the arid and semi-arid regions of the Horn of Africa could impact the grazing potential for nearly 685,000 pastoral and agro-pastoral households [6]. The United Nations Food and Agriculture Organization (FAO) reports that a large swarm covering a square kilometer can consume 200 tons of vegetation in a day causing severe impacts and destroying vital vegetation cover [7]. Earlier studies have demonstrated that DLs can cause devastating impacts in the agricultural sector, with the potential to cause between 20% and 100% losses in cropland [8–10]. These studies have shown that the pest can severely destroy both crop- and pasturelands, hence shattering food systems [10]. A DL invasion in Sahel countries in 2004 resulted in at least 8 million people suffering from immense crop damage and famine in the affected households [8]. Thus, the DL infestations caused acute food shortages, reduced grazing areas, and led to offsetting of the market prices for livestock and cereals [8]. Again, Burkina Faso, Mali, and Mauritania incurred losses of up to 90% in legume production and 80–100% in cereal production during the 2004 DL invasion. In the same period, Mali and Burkina Faso incurred a 30% loss in pastureland, while Mauritania recorded the highest loss of up to 85% in fodder production [9].

Typically, DL invasions have been observed and predicted to occur in the desert and semi-arid areas of India, Mauritania, West Africa, and the Horn of Africa, through the Middle East to Southwest Asia [6,8]. Like other insects, DLs respond to general climatic conditions where above-average rainfall leads to an increase in green vegetation cover and aboveground vegetation biomass promoting their occurrence. Further, temperature, wind, soil properties (sand content, moisture, and texture), slope and food availability contribute immensely to the pest propagation. For instance, soil physical properties influence the behavior of female DLs to lay eggs and the viability and optimal hatching time of the eggs [8]. Hence, under suitable conditions, the breeding of DLs often results in very rapid increment in their populations, leading to large concentration densities within periods of one to two months [2].

Recently in 2019, the DL invasion in the Horn of Africa raised concerns and questions over the socioeconomic well-being and livelihood sustainability in the region as well as the level of preparedness for future events. This invasion was witnessed for the first time in 70 years, spreading from Yemen, crossing over the Gulf of Aden into Djibouti, Ethiopia, Somalia, and Kenya and further into the Sahelian countries through Sudan, desolating farmlands across the Horn of Africa [11,12]. This invasion was attributed to the favorable conditions of heavy and unusual precipitation, temperature, and vegetation that supported the pest's feeding for survival and development [13]. In Kenya, the pest's implication was realized in the impact it had on most of the crop- and pasturelands. This reduced the grazing potential, which is the base of livelihood for most smallholder farmers and pastoralists in the country [14]. Essentially, damage to vegetation from this outbreak, critically weakened the socioeconomic systems of these marginalized communities in Kenya, particularly in Turkana County. Subsequently, mapping and quantifying these impacts using geospatial technologies have not been fully explored to provide critical information on the extent and time steps of the DL invasion and vegetation damage, specifically in remote and inaccessible areas. In addition, this approach affords an understanding of potential future damage to enhance the level of preparedness for such incidences.

Geospatial technologies have been successfully utilized by other studies to detect vegetation change in the arid areas of Sudan caused by DLs [15]. These earlier studies mostly relied on the moderate resolution imaging spectroradiometer (MODIS) sensors and an enhanced vegetation index (EVI) as a derivative to assess the damage caused during an infestation that confirmed a substantive amount of damage on vegetation [15,16]. Moreover, FAO relies on remotely sensed data to monitor and forecast DL outbreaks in breeding areas through vegetation greenness maps. The FAO uses satellite imagery to report on rainfall estimates and ecological conditions, such as vegetation development estimates at international and local levels, to forecast, inform early warning, and guide sustainable control measures [17,18]. Moreover, Latchininsky and Sivanpillai [18] discussed the potential applications of remote sensing and GIS in mapping locust habitats for early warning,

damage, and risk assessment using different approaches and platforms in analysing and evaluating the vegetation state.

Prediction of pest distribution based on the influence of current and future climate scenarios using machine learning techniques and remotely sensed data has been successfully used by previous studies [19–23]. These techniques have been used to inform current and future habitat distributions and the existing correlation between climate and pest distribution using environmental variables as key model predictors [24–26]. For instance, a number of species distribution models (SDMs), such as the maximum entropy (MaxEnt), random forest (RF), generalized linear model (GLM), support vector machines (SVM), etc., are widely used to predict habitat suitability of crop insect pests [11,27]. In addition, an ensemble model of several SDMs was utilized to assess pest (e.g., DL) habitats and establishment sites. The MaxEnt model, which is the most widely used SDM, has demonstrated reliable predictions of species habitats using a small sample size compared to other models, i.e., genetic algorithm for rule-set prediction (GARP) [28]. Moreover, MaxEnt uses presence-only species records and correlates them to a set of relevant environmental variables in determining the habitat suitability of the species under study [29]. Likewise, other process-based models, such as CLIMEX, are used to predict pest risks [30].

Furthermore, the abovementioned studies have utilized 16-day MODIS products recorded at 250 m spatial resolution to study vegetation states at regional extents. However, the accuracy of detecting vegetation state depends largely on the pixel size, hence utilizing MODIS products would result in inaccurate vegetation detection at 250 m spatial resolution, particularly when the vegetation in some DL habitats is sparse [15,16]. On the other hand, using 5-day Sentinel-2 imagery that is of a medium spatial resolution (10 m) would improve the accuracy and reliability in assessing vegetation damage compared to the MODIS products [31]. Therefore, this study aimed to use relatively recent and moderate spatial resolution remotely sensed data and geospatial modelling techniques to assess the potential DL risk of invasion (current and future) and vegetation damage using Turkana County in Kenya as a case study. We computed NDVI for the period of 2018–2020, which was a period that experienced good rainfall during the long rainy season in Kenya, particularly in 2019–2020. Therefore, it was not anticipated that any abiotic stress, such as drought, could have caused a reduction in NDVI in Turkana County. The long rainy season in 2020 coincided directly with the DL upsurge. Therefore, we hypothesized that any decline in NDVI could be due to DL damage owing to the massive invasion and the devastating feeding pattern of the pest.

## 2. Methods

### 2.1. Study Area

This study was conducted in Turkana County (Figure 1), a semi-arid region in north-western Kenya covering approximately 68,232.9 km<sup>2</sup> with a population of 926,976 people and an annual population growth rate of 0.81% [32]. Turkana lies between latitudes of 1°30′00″ N and 5°30′00″ N and longitudes of 34°30′00″ E and 36°40′00″ E. The elevation in the study area ranges between 369 m around Lake Turkana and 900 m above sea level located at the border between Kenya and Uganda. Administratively, the study area is divided into six sub-counties; Turkana North, Turkana Central, Turkana South, Turkana West, Turkana East, and Loima [33].

The region has a bimodal rainfall pattern with ‘long rains’ occurring during the period between April and July and ‘short rains’ occurring between October and November [34]. On average, yearly precipitation ranges between 52 mm and 480 mm with an annual average of 200 mm. The annual temperature range is between 20 °C and 41 °C with an annual mean of 30.5 °C [33]. The county is susceptible to drought with 80% of the total area considered either arid or semi-arid, with the driest periods occurring in January, February, and September [33].

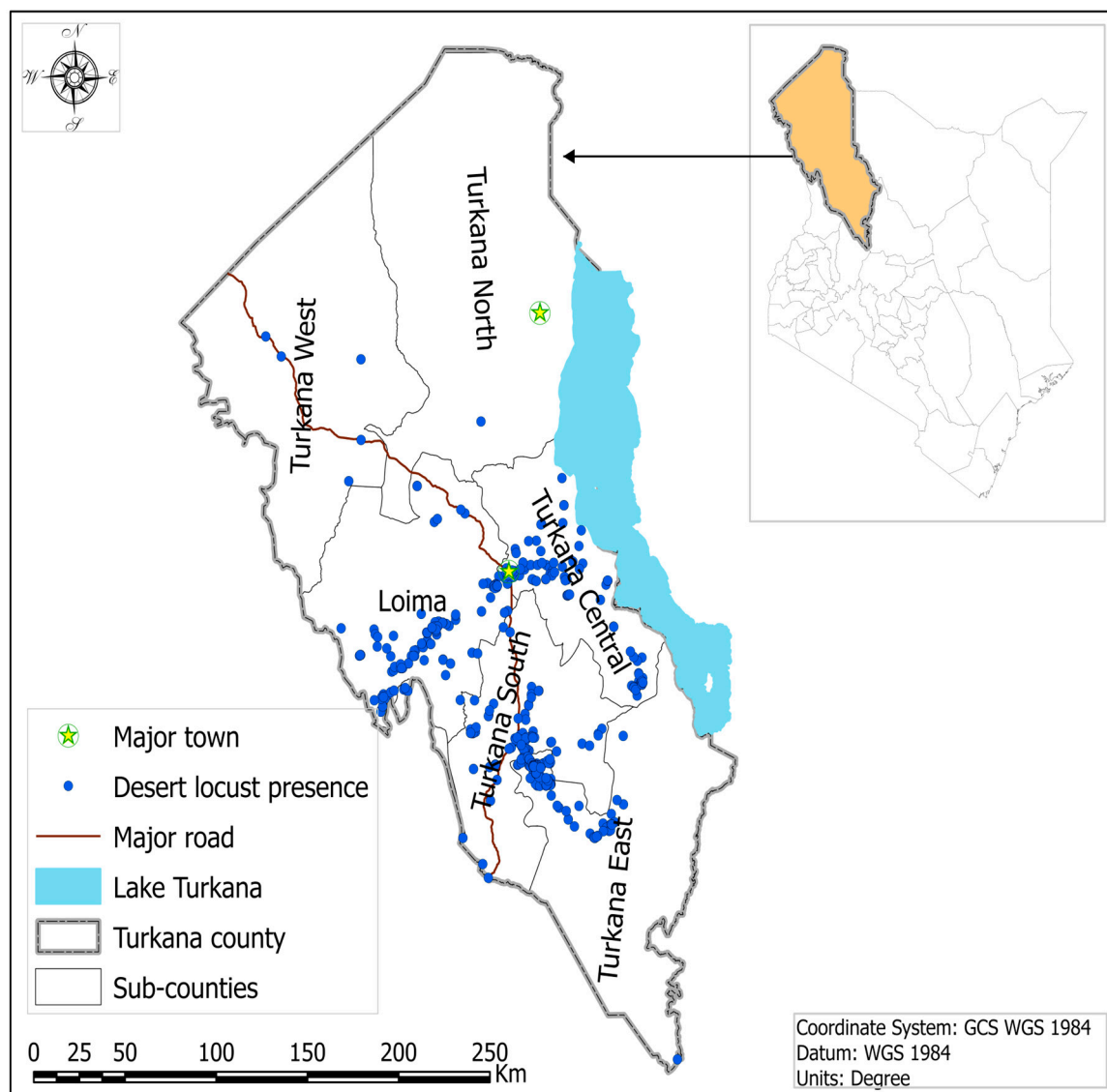


**Figure 1.** Location of Turkana County in Kenya and locations of the six sub-counties in Turkana.

The vegetation characteristics in the study area are diverse, ranging from patchy grassland, herbaceous plants combined with shrubs, and riverine woody species [35–37]. Additionally, the area is dominated by dwarf shrubs, bushy tree species, and riverine vegetation along the main rivers [30,31,38]. Furthermore, *Acacia reficiens* and *Acacia melifera* are the most dominant and critical forage tree species for animal browsing in the study area, while *Aristida mustabilis* and *Cenchrus ciliaris* are the most common annual and perennial pasture species [31–33]. On the other hand, invasive tree species, such as *Prosopis juliflora*, are also densely distributed in the region outcompeting the herbaceous plants that grow under their canopy [30,31,34].

## 2.2. Data Acquisition and Processing

The data considered in this study included Sentinel-2 (S2) imagery, DL occurrence observations, and bioclimatic predictor variables. The S2 imagery was used in this study because it provides relatively moderate spatial resolution (10 m × 10 m), which is considered by other studies as one of the best satellite data sources for assessing vegetation damage and change [39,40]. Additionally, S2 data are freely and readily available, making them more useful in resource-restrained regions such as Kenya. Future climate scenarios of the shared socioeconomic pathways (SSP) that are projected by the coupled model

intercomparison project version 6 (CMIP6) were used in this study to represent the future climate scenarios [41], whereas the DL occurrence data were obtained from the FAO DL hub (<https://locust-hub-hqfao.hub.arcgis.com/> accessed on 10 June 2021). Furthermore, climatic data from the national aeronautics and space administration (NASA) prediction of worldwide energy resources (<https://power.larc.nasa.gov/> accessed on 10 June 2021) were analyzed to provide a baseline in weather trends for the study period, i.e., 2018 to 2020.

### 2.3. Sentinel-2

Multi-date S2 imagery was acquired and analyzed in Google Earth Engine (GEE) for the period 2018, 2019, and 2020 in May, June, and July ( $n = 771$  scenes). The S2 imagery is provided by the European Space Agency (ESA) with a 5-day revisit time at the equator and 2–3 days at mid-latitudes collected from two satellite sensors, i.e., S2A and S2B. These two S2 sensors provide 13 spectral bands (Table 1), each of varying pixel size of 10 m (at visible: blue, green, and red bands), 20 m (at infrared: red edge 1, red edge 2, and red edge 3, narrow near-infrared, shortwave infrared 3, and shortwave infrared 4 bands) and 60 m (at water vapor: shortwave infrared 1, and shortwave infrared 2 bands) at a swath width of 290 km<sup>2</sup>. In this study, we used the level 1C of the S2 product, which is a top-of-the-atmosphere (TOA), orthorectified imagery. The size of each image was 100 km × 100 km, projected into the Universal Transverse Mercator (UTM)/WGS84. Furthermore, the median mosaicking approach for 771 scenes that had less than 20% cloud cover was used to generate the image data used in the analysis. Only the red (band 4) and near-infrared (band 8) were selected to calculate the normalized difference vegetation index (NDVI) that was used as a proxy for vegetation coverage and density in the study area. Specifically, the first 10 S2 images of every month matching the “long rain” season, i.e., when vegetation productivity and level of greenness were expected to be above average and coincided with the time of the invasion of DLs in 2020 in Turkana County, were used.

**Table 1.** Sentinel-2 multispectral sensor bands, description, wavelength, and their respective pixel size. The bold, i.e., bands 4 (Red) and 8 (NIR) were the only bands used in this study.

| Band      | Band Description                        | Central Wavelength (nm) | Pixel Size (m) |
|-----------|---|-------------------------|----------------|
| B1        | Coastal aerosol                         | 443                     | 60             |
| B2        | Blue                                    | 490                     | 10             |
| B3        | Green                                   | 560                     | 10             |
| <b>B4</b> | <b>Red</b>                              | <b>665</b>              | <b>10</b>      |
| B5        | Red-edge 1 (RE1)                        | 705                     | 20             |
| B6        | Red-edge 2 (RE2)                        | 740                     | 20             |
| B7        | Red-edge 3 (RE3)                        | 783                     | 20             |
| <b>B8</b> | <b>Near-infrared (NIR)</b>              | <b>842</b>              | <b>10</b>      |
| B8a       | Narrow NIR (NNIR)                       | 865                     | 20             |
| B9        | Short wave infrared (SWIR1)-water vapor | 940                     | 60             |
| B10       | Short wave infrared (SWIR2)-cirrus      | 1375                    | 60             |
| B11       | Short wave infrared (SWIR3)             | 1610                    | 20             |
| B12       | Short wave infrared (SWIR4)             | 2190                    | 20             |

### 2.4. Daily Climatic Data in the Study Area

Monthly average precipitation and temperature data were obtained from NASA’s prediction of worldwide energy resources (<https://power.larc.nasa.gov/>, accessed on 10 June 2021) to analyze monthly weather trends in the period 2018 to 2020. Monthly temperature (°C) at 2 m above the ground surface and monthly precipitation (mm·month<sup>−1</sup>) both at 0.5 × 0.5 degrees (55 × 55 km) resolution were visualized in R-software [42] using the ggplot2 package [43]. These data were explored to demonstrate and relate the weather conditions that prevailed during the period of DL invasion (May, June, and July 2020) in the study area (Figure 2).



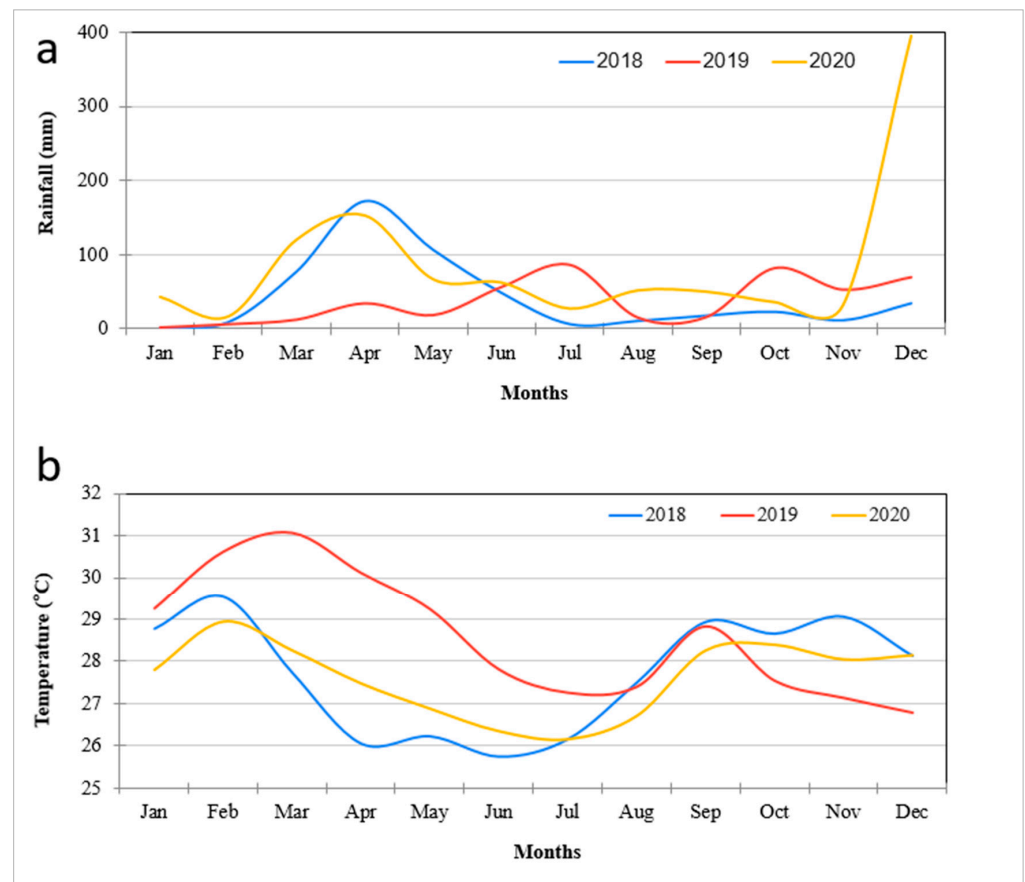


**Figure 2.** (a) Monthly mean precipitation and (b) temperature for Turkana County from 1 January 2018 to 31 December 2020.

### 2.5. Desert Locust (DL) Occurrence Data

Freely available data on DL occurrence were acquired from the FAO DL hub (<https://locust-hub-hqfao.hub.arcgis.com>, accessed on 10 June 2021). Data of the DLs at the adult stage were used in this study because they cause severe damage to vegetation compared to other stages of development, e.g., the hoppers stage. The DL occurrence data that were collected between 1 February and 31 August 2020 were used. This period coincided with the peak populations and DL invasion in the East African region [11]. However, we selected May, June, and July as the study months because these were the months that were reported to have recorded the highest DL populations and the largest invasion spatial extent in the region. The data underwent rigorous cleaning for redundancy and positional accuracy using R-software and Google Earth, respectively to remove duplicates and outliers. After this elimination process, a total of 646 data points were retained from an initial 847 data points obtained from the FAO DL database. Even though spatial thinning is a necessary process that addresses problems associated with spatial sampling bias, it was not considered in this study, because the data were assumed free from sampling bias as the DL observations were collected at different periods representing an occurrence in space and in time. Hence, we needed to retain the data for a widespread spatiotemporal representation, such an approach was performed in earlier studies [8,44].

### 2.6. Bioclimatic Data

Table 2 illustrates the 19 bioclimatic variables that were used to predict the current and future potential habitat distribution of DLs. These current and future bioclimatic variables were obtained from the Worldclim2 database ([www.worldclim.org](http://www.worldclim.org), accessed on 10 June 2021) [45]. The bioclimatic data from WorldClim (version 2.1) used in this

study comprised monthly minimum, maximum, mean temperature, and precipitation variables [45].

**Table 2.** The 19 bioclimatic variables that were considered in the desert locust distribution modelling. The bold variables were used in the final analysis after the elimination of the correlated variables accessed on 10 June 2021.

| Bioclimate Code | Variable Description                        | Unit |
|-----------------|---|------|
| <b>Bio1</b>     | <b>Annual mean temperature</b>              | °C   |
| <b>Bio2</b>     | <b>Mean diurnal range</b>                   | °C   |
| Bio3            | Isothermality                               | NU * |
| <b>Bio4</b>     | <b>Temperature seasonality</b>              | NU * |
| Bio5            | Max temperature of warmest month            | °C   |
| Bio6            | Min temperature of coldest month            | °C   |
| Bio7            | Temperature annual range                    | °C   |
| Bio8            | Mean temperature of wettest quarter         | °C   |
| Bio9            | Mean temperature of driest quarter          | °C   |
| Bio10           | Mean temperature of warmest quarter         | °C   |
| Bio11           | Mean temperature of coldest quarter         | °C   |
| <b>Bio12</b>    | <b>Annual precipitation</b>                 | mm   |
| Bio13           | Precipitation of the wettest month          | mm   |
| Bio14           | Precipitation of the driest month           | mm   |
| <b>Bio15</b>    | <b>Precipitation seasonality</b>            | NU * |
| Bio16           | Precipitation of the wettest quarter        | mm   |
| Bio17           | Precipitation of the driest quarter         | mm   |
| <b>Bio18</b>    | <b>Precipitation of the warmest quarter</b> | mm   |
| Bio19           | Precipitation of coldest quarter            | mm   |

\* NU = no unit

The current environmental variables were obtained at 30 s (1 km) spatial resolution, and future climatic scenarios from the model for interdisciplinary research on the climate (MIROC 6) model [46] were acquired at 2.5 min (5 km) spatial resolution. The “resampling” function of the raster package in R [38,42] was used to attain spatial homogeneity where future climatic scenarios at 5 km were resampled to 1 km, retaining pixel information with current scenarios as the baseline [47,48]. A collinearity test was performed on the 19 bioclimatic variables using the “virtual species” package in R-software to explore the clusters of the spatial correlation of the 19 bioclimatic variables [49]. Correlated variables were clustered into 6 groups ( $r \geq 0.70$  Pearson correlation coefficient), and 1 predictor variable with the least correlation value in each cluster was selected for use in the DL habitat distribution model experiment [49]. The 6 bioclimatic variables that were retained and used in developing the model from this collinearity were Bio 1 (annual mean temperature), Bio 2 (mean diurnal range), Bio 4 (temperature seasonality), Bio 12 (annual precipitation), Bio 15 (precipitation seasonality), and Bio 18 (precipitation of warmest quarter).

The future bioclimatic variables are based on two narratives of SSPs. The SSPs provide narratives describing alternative socioeconomic developments with intermediate greenhouse gases emission (GHG) SSP2-4.5 (middle of the road) and very high GHG emission SSP5-8.5 (fossil fueled development) were used to predict the current and future potential geographic distribution of DLs [50]. The SSPs scenarios represent the middle of the road and the highest radioactive forcing of  $4.5 \text{ W/m}^2$  and  $8.5 \text{ W/m}^2$ , respectively, for the carbon dioxide ( $\text{CO}_2$ ) concentration for the period 2021–2040 averaged at 2030 [51].

## 2.7. Vegetation Damage Analysis Using the Normalized Difference Vegetation Index (NDVI)

The multitemporal normalized difference vegetation index (NDVI) analysis was performed across the three study years (2018, 2019, and 2020) to assess the general condition of vegetation in the study area. Monthly analysis was performed to determine vegetation damage during the peak of DL infestation. Three months of May, June, and July that coincided with the “long rains” season and the DL outbreak in the area were selected to

check against optimal vegetation greenness. The NDVI is an indicator that can be used to estimate the quantity of green vegetation over an area using the magnitude of greenness [52]. The index utilizes the reflectance at the near-infrared (NIR) and visible red bands to analyze vegetation conditions using a normalized band ratio as shown in Equation (1). The NDVI values that are close to zero indicate reflectance from rocks and bare soil, while water, clouds, and snow have negative index values attributable to a higher reflectance in visible red than NIR [47–50]. Sparse vegetation could have values of 0.2–0.3, and densely vegetated areas have value ranges between 0.4 to 0.8 [53].

The NDVI analysis was computed in the GEE cloud-based platform for spatial and temporal geoprocessing since it possesses high computation capabilities over a large dataset [54–56]. A median compositing approach was used over the time series imagery, thereby reducing the huge image collection dataset into an individual image across the selected months for each of the years 2018, 2019, and 2020. In this case, the output was a product of a median value from all the images in the collection across the month at a location computed in each pixel [57–59]. Nine NDVI maps (three for each year) were generated and exported for further processing in Quantum GIS (QGIS) software, version 3.18.0. The mosaicking function was used to generate a single composite image for the entire study area to facilitate seamless analysis.

$$\text{NDVI} = \frac{(\text{PNIR} - \text{PR})}{(\text{PNIR} + \text{PR})} \quad (1)$$

where

NDVI = normalized difference vegetation index,

PNIR = near-infrared reflectance, and

PR = red reflectance.

The NDVI image was categorized into three classes, i.e., (i) low (−1.0 to 0.2), (ii) moderate (0.2 to 0.5), and (iii) high (0.5 to 1.0) following [59]. In 2020, for vegetation damage analysis (i.e., months of May, June, and July), the NDVI was categorized into values less than 0.2 to indicate high vegetation damage, values between 0.2 and 0.5 to indicate moderate vegetation damage, and values more than 0.5 as low vegetation damage.

During the study months, the study area did not witness any drought or dry spells that might have affected the vegetation performance in the study area; hence, we hypothesized that the decrease in the vegetation greenness, density, and cover was largely due to DL damage. Therefore, we compared the areas that showed high (hotspots) and no vegetation changes with the DL occurrence and density observations to obtain insights into the effect of DLs on vegetation damage in Turkana County.

## 2.8. Current and Future Desert Locust Invasion Risk Analysis

We utilized the MaxEnt model (MaxEnt version 3.4.4) [29] to predict the current and future distribution of DLs in the study area. The MaxEnt model uses presence-only data and has been reported by other studies to provide higher predictive performance in modelling species habitat suitability compared to other machine learning methods [8,23,26,56,60]. The MaxEnt algorithm estimates a probability of distribution of species occurrence that is most spread against environmental constraints and does not require a high number of observations [28,61].

The variable contribution to the model was compared using the Jackknife test [61,62]. The ‘ENMevaluate’ function in the package ‘ENMeval’ [63] available in R-software [42] was used to find the most optimum parameters for the MaxEnt model. The ‘ENMevaluate’ function aids in the empirical selection of the best model settings that balance goodness-of-fit and model complexity and calculates multiple metrics using the presence-only reference points of the species being analyzed [60,61,64]. In this study, the optimum model parameters derived from the ‘ENMevaluate’ were linear/quadratic/product/hinge (LQPH): 0.050, categorical: 0.250, threshold (H): 1.000, hinge: 0.50, and beta-multiplier: 3.0. Initially, we



ran the MaxEnt model with the default parameters which resulted in an overfitting model; therefore, we sought for optimum values using the 'ENMevaluate' tool. QGIS software was used to categorize the DL potential distribution maps into five suitable habitat scores, which were determined based on [65]. Specifically, the potential DL distribution classes (i.e., suitable habitat scores) were regrouped into 5 categories as follows: (i) 0–0.2 (very low), (ii) 0.2–0.4 (low), (iii) 0.4–0.6 (moderate), (iv) 0.6–0.8 (high), and (v) 0.8–1.0 (very high).

### 2.9. Ecological Niche Modelling Performance Validation

The receiver operating characteristic (ROC) was employed to calibrate and determine the robustness of the MaxEnt model [19]. The area under the curve (AUC) of the ROC was further used to examine and estimate the model performance. The AUC values range from 0 (random prediction) to 1 (perfect prediction) [22,26]. We used 70% ( $n = 258$ ) of the DL occurrence data to train the model, while 30% ( $n = 65$ ) were used to test the performance of the predicted modelling outputs [8,55]. A 5-fold cross-validation approach with 10,000 background points and 500 iterations was used to evaluate the precision of the model [22,62,66]. In addition, the true skill statistic (TSS) which is based on the components of the standard confusion matrix representing matches and mismatches between observations and predictions was used to evaluate the accuracy of the model by calculating the sensitivity and specificity of the models ( $TSS = sensitivity + specificity - 1$ ). The TSS was calculated for all the five model replicates, and a mean TSS score was determined. The TSS values range from  $-1$  to  $1$  with negative and  $0$  values suggesting a random prediction, while values close to  $1$  indicating agreement between predictions and observations [26].

## 3. Results

### 3.1. Vegetation Damage Analysis

In 2018, vegetation greenness was relatively low across the three months of May, June, and July. Most parts of the study area indicated low vegetation greenness in May, which further reduced in June and July, particularly in the northern regions of Turkana, which indicated very low NDVI values (Figure 3).

Comparatively, in 2019, an increase in vegetation greenness was observed across the three months compared to 2018 (Figure 3). It was also observed that areas around the borders of Uganda and South Sudan showed an increase in vegetation greenness across the three study months peaking from May through July compared to central regions and regions along the shoreline of Lake Turkana (Figure 3). The northern and southern parts towards the borders of the county demonstrated an increase in vegetation greenness. These parts exhibited high vegetation performance in July compared to June with a moderate vegetation performance in most of those areas.

In 2020, the analysis revealed that vegetation greenness performance was much better across the three months compared to the previous years of 2018 and 2019. However, a comparison across the months in 2020 showed that May recorded relatively higher vegetation greenness compared to June. In July, a slight increase in vegetation greenness was observed as opposed to June.

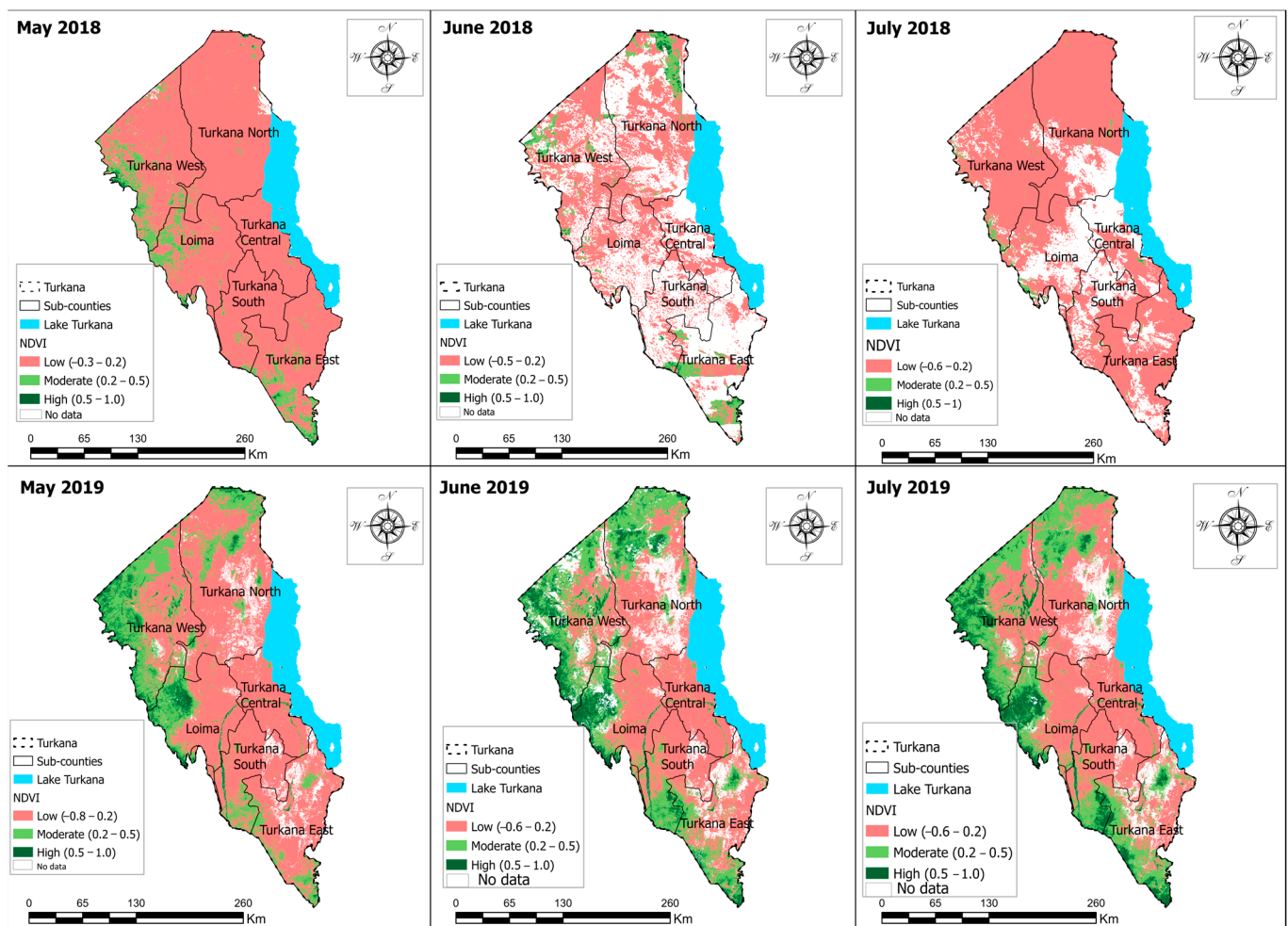


**Figure 3.** Level of vegetation greenness represented by the normalized difference vegetation index (NDVI) for May, June, and July 2018 and 2019.

#### Monthly Normalized Difference Vegetation Index (NDVI) Trend and Vegetation Damage for the Period May–July 2020

The highest NDVI recorded in May 2020 was 0.61 at the start of the second week. A varying degree of vegetation greenness in a decreasing trend across May and constant greenness at the end of the second week recorded a low NDVI value of 0.36 with an increase at the end of the third week (Figure 4a). In June, the NDVI values were comparatively low with a decreasing trend in the second week and towards the third week of the month, which recorded a low NDVI value of 0.22 (Figure 4b). Moreover, a higher NDVI of 0.59 was recorded at the start of the fourth week of June followed by a decrease in July to the lowest NDVI of 0.24. A varying trend in greenness into July was observed with the first week of the month indicating a decreasing trend with a low NDVI of 0.18 and a sharp increase into the second week recording the highest NDVI of 0.53 (Figure 4c). A decline was recorded at the end of the second week towards the third week at 0.10 with a slight increase in the fourth week. There was also a fairly constant and possible increase in NDVI towards August. Nonetheless, May performed slightly better than June and July, which recorded relatively low greenness.

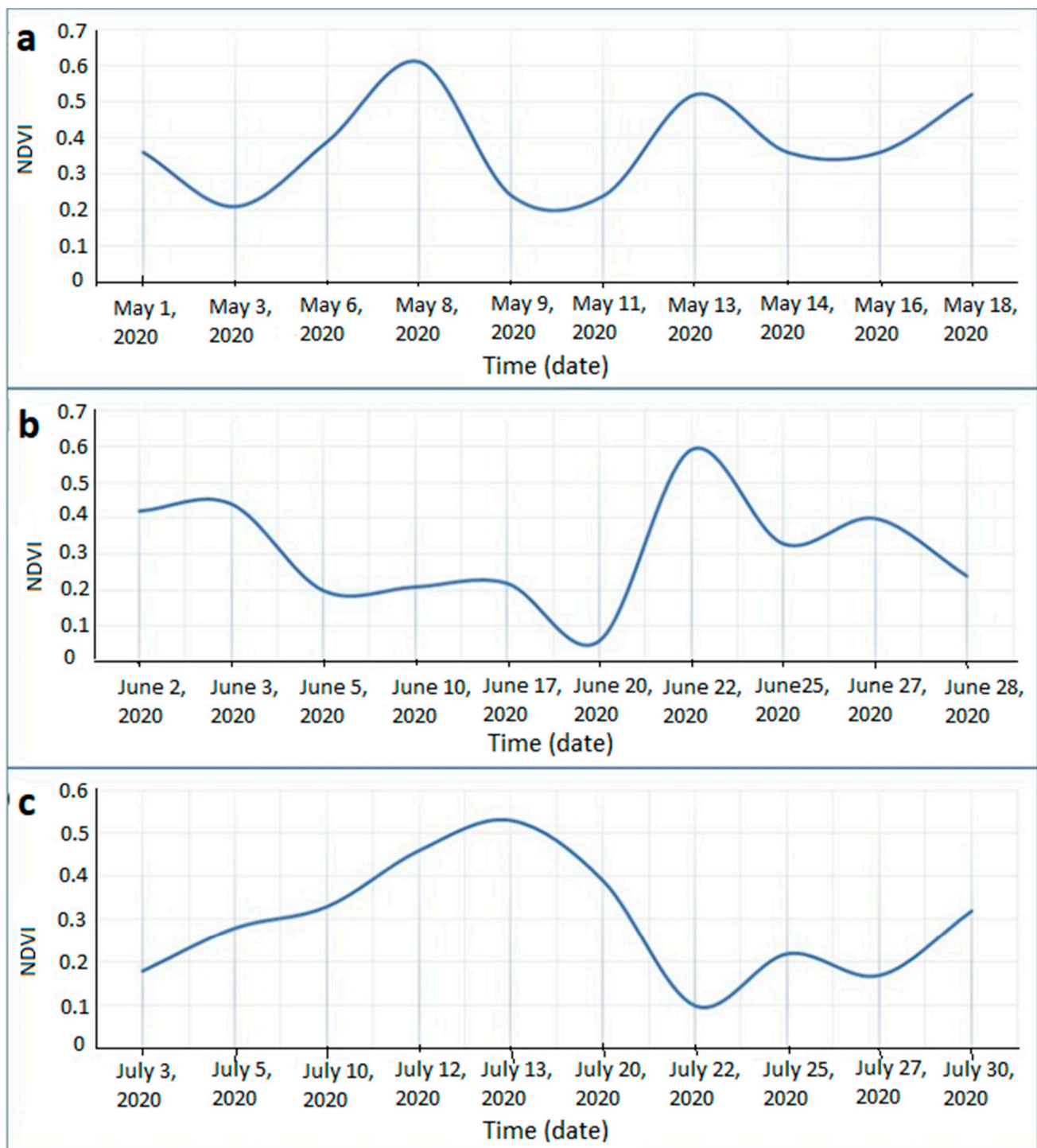


**Figure 4.** Normalized difference vegetation index (NDVI) trend in Turkana County, Kenya in May (a); June (b); and July (c) 2020. These three months were the peak desert locust infestation period in the county in 2020.

In general, the vegetation greenness across the three months was on a decreasing trend. May showed the highest vegetation greenness with June and July indicating a further decrease in different areas in the county (Figures 5–7). In May, in the sub-counties of Loima, Turkana East, Turkana Central, and Turkana West, the vegetation damage was moderate to high. The vegetation reduction in these sub-counties was assumed to be a result of DL infestations, which were reported in these areas. This trend was further

continued in the subsequent months of June and July, where the DL-infested sub-counties demonstrated NDVI values of less than 0.5, implying moderate to high vegetation damage. Furthermore, Loima, Turkana South, and Turkana East consistently recorded a high number of DL observations with Turkana West and Central recording low records across the three months (Figures 5–7). However, the northern parts showed considerable moderate to high vegetation damage despite the low DL observations records. This is an indication of a possibility of no surveillance due to inaccessibility and lack of resources.

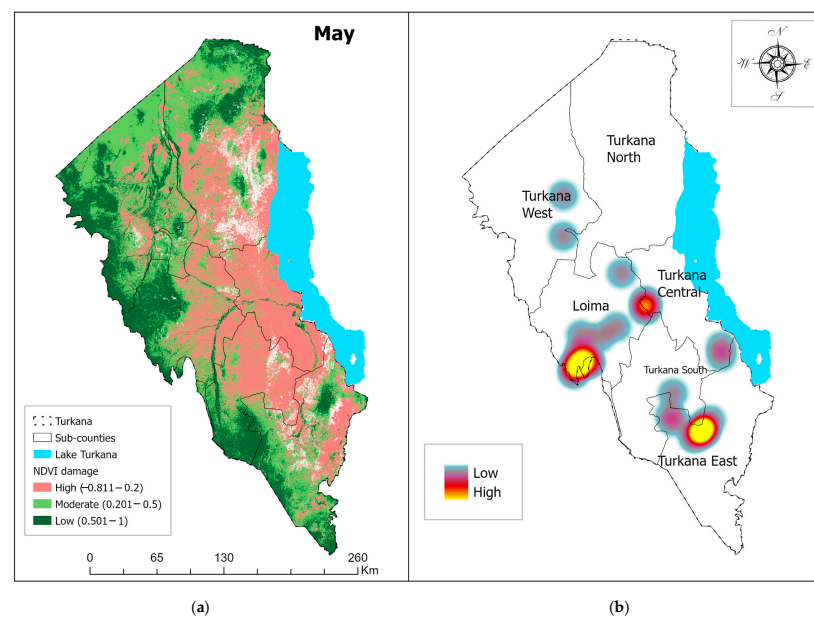


**Figure 5.** Vegetation damage assessment indicated by (a) the normalized vegetation index (NDVI) and (b) desert locust occurrence records for May 2020 in Turkana County in Kenya. The dark green color shows areas of low vegetation damage, light green and pale red show areas with moderate and high vegetation damage, respectively.

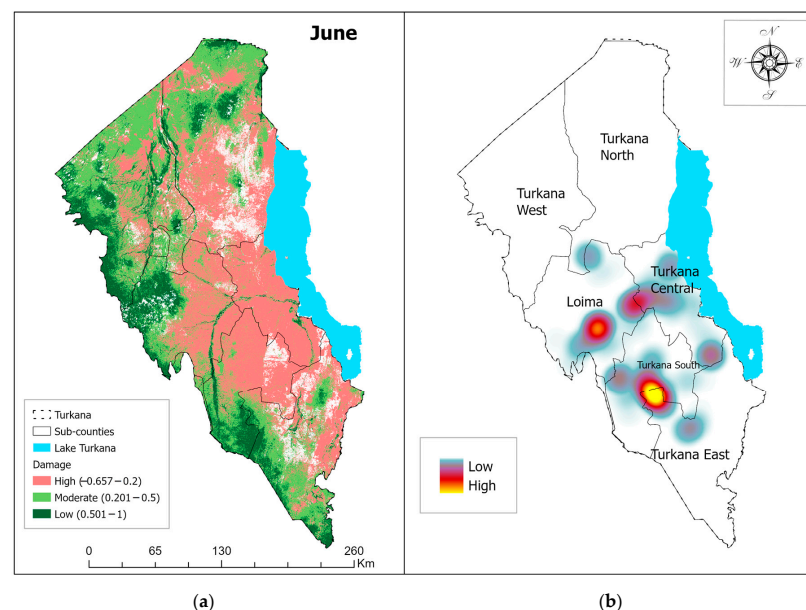


**Figure 6.** Vegetation damage assessment indicated by (a) the normalized vegetation index (NDVI) and (b) desert locust occurrence records for June 2020 in Turkana County in Kenya. The dark green color shows areas of low vegetation damage, light green and pale red show areas with moderate and high vegetation damage, respectively.



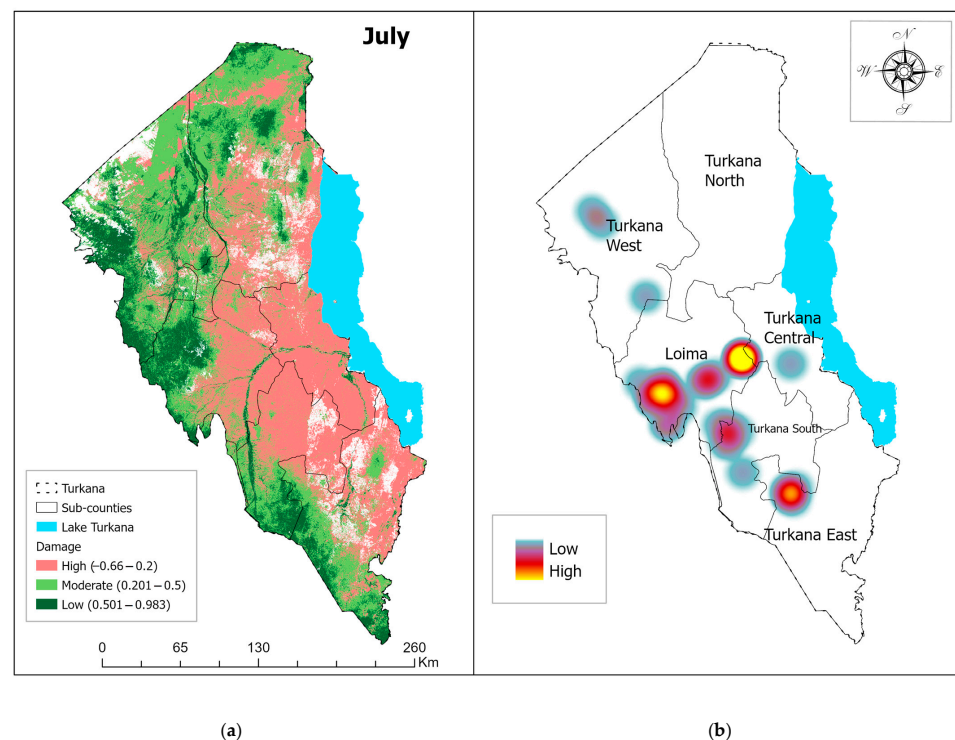


**Figure 7.** Vegetation damage assessment indicated by (a) the normalized vegetation index (NDVI) and (b) desert locust occurrence records for July 2020 in Turkana County in Kenya. The dark green color shows areas of low vegetation damage, light green and pale red show areas with moderate and high vegetation damage, respectively.

### 3.2. Current and Future Desert Locust Invasion Risk

#### 3.2.1. Maximum Entropy (MaxEnt) Model Evaluation

The MaxEnt model for predicting DL habitat suitability and invasion risk achieved high AUC values of  $0.87 \pm 0.009$  (Figure 8) and TSS of 0.61, which were greater than a threshold of 0.5 indicating a high model performance.

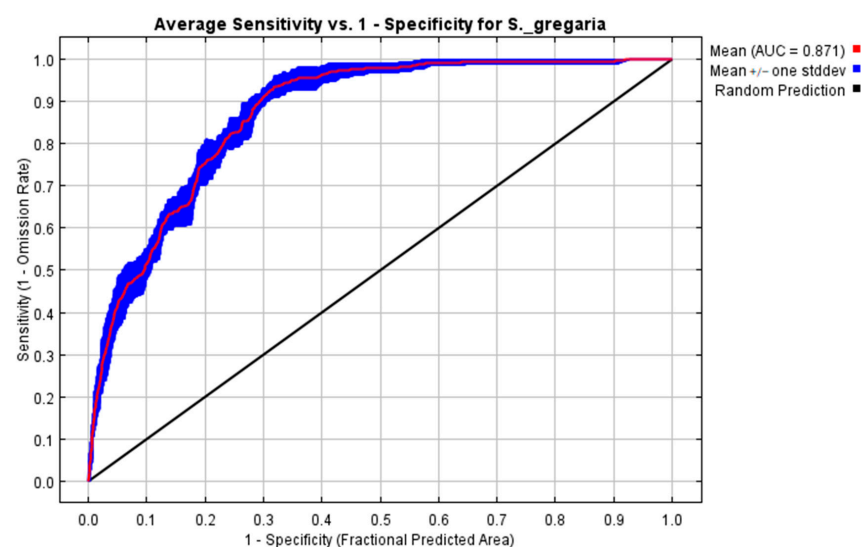


**Figure 8.** Maximum entropy (MaxEnt) model validation using area under the curve (AUC) showing the model performance in predicting desert locust invasion risk in Turkana County. The red line indicates the mean AUC value for the MaxEnt replicates, while the blue shades show the AUC standard deviation on the model replicates, and the black line indicates the performance of the model using random predictions.



### 3.2.2. Predictor Variable Contribution on the Maximum Entropy Model

The Jackknife test result (Figure 9) illustrated the various bioclimatic variables' contribution (%) towards predicting DL habitat suitability. Bio 4 (temperature seasonality) contributed the most (83.10%) to the DL distribution in Turkana County, followed by Bio 2 (mean diurnal range), and Bio 18 (precipitation of the warmest quarter), respectively (Table 3). In general, temperature-based variables were more important than the precipitation variables in predicting DLs in Turkana County. Moreover, the Bio 4 variable demonstrated the highest gain in the MaxEnt model when utilized in isolation and the lowest gain when omitted from the MaxEnt modelling experiment (Figure 9).

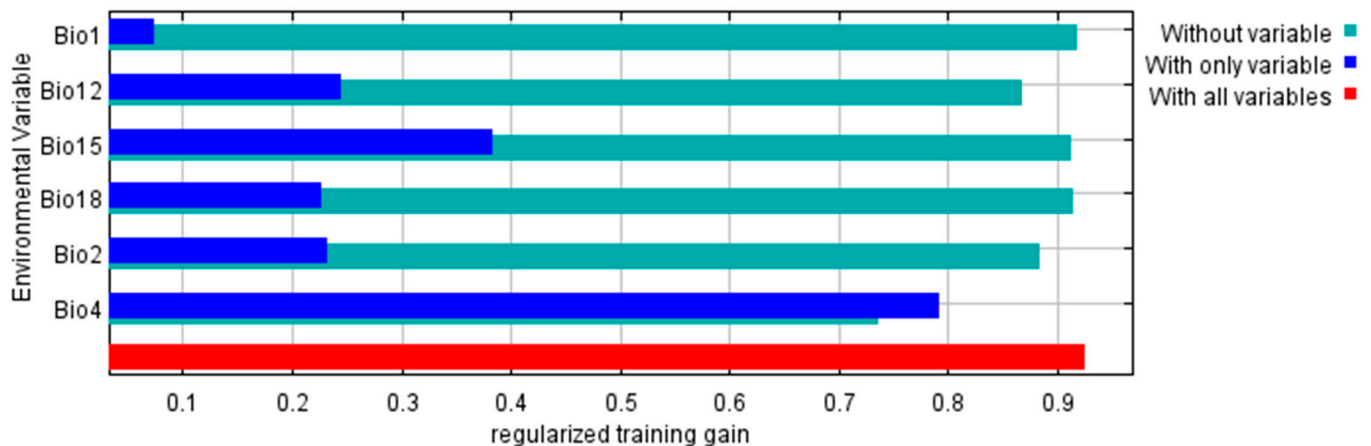


**Figure 9.** Jackknife test assessing bioclimatic variable importance for predicting desert locust invasion risk in Turkana County, Kenya. Red bars show model performance with all bioclimatic variables, blue bars indicate model performance when only one corresponding variable was used, and torques bars present model performance without variables.

**Table 3.** The relative contribution of the six bioclimatic predictor variables utilized in the maximum entropy (MaxEnt) model to predict the current and future invasion risk of desert locusts in Turkana County, Kenya.

| Bioclimate Code | Variable Description                 | Contribution (%) |
|-----------------|--------------------------------------|------------------|
| Bio4            | Temperature seasonality              | 83.1             |
| Bio2            | Mean diurnal range                   | 4.8              |
| Bio18           | Precipitation of the warmest quarter | 4.0              |
| Bio12           | Annual precipitation                 | 3.9              |
| Bio15           | Precipitation seasonality            | 2.4              |
| Bio1            | Annual mean temperature              | 1.7              |

### 3.2.3. Predicted Current Desert Locust Invasion Risk

The MaxEnt model predicted sub-counties of Turkana Central, Turkana South, Loima, and parts of Turkana East to be at the highest risk as they provide the most suitable habitats for DLs under the current (2020) climatic conditions (Figure 10a). Turkana East was predicted to have low to moderately suitable habitats to the south with patches of very low suitability scattered in the area. Turkana North and Turkana West indicated patches of low habitat suitability near the borders of Loima and Turkana Central sub-counties with large portions of very low habitat suitability evenly distributed across the two sub-counties. Generally, the northern part of Turkana was predicted to be unsuitable for DLs, and the central sub-counties were predicted to be highly to very highly suitable, with low suitability in the south of the area (Figure 10a).

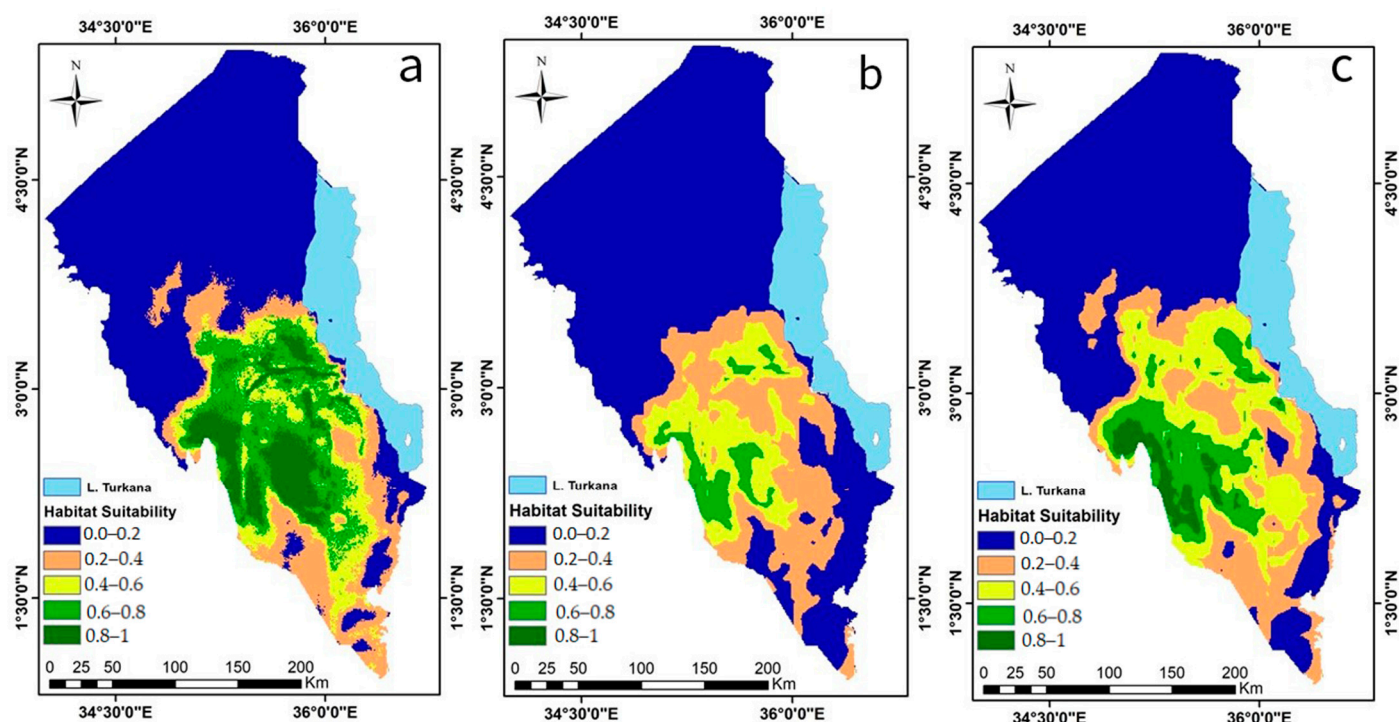


**Figure 10.** Predicted habitat suitability for desert locust invasion in Turkana County, Kenya: (a) in the current (2020); (b) future under the SSP2-4.5 scenario; and (c) future under the SSP5-8.5 scenario.

#### 3.2.4. Predicted Potential Future Desert Locust Invasion Risk

Future (2030) DL prediction (Figure 10b,c) showed relative similarity in distribution when contrasted with the current distribution prediction; however, a decrease in the suitability and invasion risk range for both SSP2-4.5 and SSP5-8.5 scenarios was noted. Additionally, SSP2-4.5 showed relatively low DL habitat suitability at 23.58% compared to SSP5-8.5, which predicted an increase in suitability range at 35.17%. In SSP5-8.5, there was a shift in habitat suitability concentration towards the edge of Loima and Turkana South sub-counties with high to very high habitat suitability. In both scenarios, in the northern sub-counties of Turkana West and Turkana North, the suitability range was relatively low. For SSP5-8.5, the habitat suitability range remained the same compared to the current predicted conditions. However, a decrease in habitat suitability levels was observed with large portions predicted to range from low to moderately suitable. Moreover, for SSP2-4.5, the geographical range was limited to low and moderate suitability with a decreased DL habitat coverage by 2030. The optimal habitat suitability (0.6–1.0) under the SSP2-4.5 scenario will decrease to 9.25%, and the SSP5-8.5 scenario will decrease to 20.34% from the current suitability of 27.15% of the total area (Table 4).

**Table 4.** Area and percentage of optimal desert locust habitat suitability for invasion (0.6–1.0) for current and future (2030) climate scenarios.

| Period  | Climate Scenario<br>(MIROC 6 Climate Model) | Area (km <sup>2</sup> ) | Percentage of the<br>Total Area |
|---------|---|-------------------------|---------------------------------|
| Current |   | 18,937.67               | 27.15                           |
| 2030    | SSP2-4.5                                    | 6455.62                 | 9.25                            |
|         | SSP5-8.5                                    | 14,192.74               | 20.34                           |

## 4. Discussion

### 4.1. Vegetation Change Analysis

This study highlighted the change in vegetation across May, June, and July of 2018, 2019, and 2020 using S2 multispectral imagery at a medium spatial resolution of 10 m.

These three months were targeted as they represented the peak of DL invasion in the study area in 2020. Thus, this study aimed to use relatively recent and moderate spatial resolution remotely sensed data and geospatial modelling techniques to assess the potential DL risk of invasion (current and future) and vegetation damage in Kenya using Turkana County as a case study.

The NDVI derived from the S2 remotely sensed data was used to assess the vegetation dynamics in the study area, and it was assumed that during the study months, there was no drastic vegetation damage from confounding factors, such as drought, which could have also led to vegetation loss. The study area often experiences dry conditions, which make it challenging to clearly distinguish and separate other vegetation loss drivers from the losses incurred by DL attacks. However, the selected period (May–July 2020) in this study demonstrated good rainfall patterns that persisted from the short rains received in October–December 2019 up to July 2020 (Figure 2). These observed patterns resulted in enhanced vegetation greenness that made it possible to estimate vegetation cover losses and establish relationships between vegetation and the locust attack in 2020.

The study demonstrated that the S2-generated NDVI can provide an estimate of vegetation dynamics due to DL infestation at both local and regional scales. The NDVI has been used in many studies as a key proxy to measure overall vegetation greenness performance [67]. However, satellite imagery is subject to atmospheric noise and cloud cover, which makes it challenging to perform an accurate vegetation analysis. This caused data gaps in certain periods, such as in our case, where the target months (May, June, and July) had missing information at some locations in the study area. The problem was overcome through the performance of the median image composite and cloud masking in GEE, which improved the reliability and usage of our imagery. This is a relatively recent common procedure for reducing cloud effects and outliers in satellite imagery data [68].

Furthermore, the NDVI analysis showed variation in vegetation greenness across the years with 2018 demonstrating low levels of vegetation greenness compared with 2019 and 2020. This progressive increment in vegetation greenness is attributed to an improved amount of precipitation across the study years 2019–2020 [69]. A good vegetation greenness performance was observed in the period 2019–2020, which was an indication of vegetation recovery from 2018 due to a fair amount of rainfall in the long rainy season (March–May) in the study area. In 2020, the vegetation greenness was high compared to the previous years, an indication of good and unusual rains received from the short rainy season in October–December 2019 extending to the long rainy season in March–May 2020 [70–72]. Precipitation is positively correlated with vegetation performance over space and time [68,69]. This could have been what triggered the mass invasion by the DLs in Kenya.

Despite the good rains received in the off-season (i.e., the short rainy season), NDVI monthly change analysis indicated a decreasing trend in vegetation performance from May to July 2020. As expected, this period coincided with the vegetative stages of crops and pasture, which are translatable to high NDVI values. Therefore, the damage in vegetation observed in June compared to May and July 2020 could be highly attributed to the huge swarms of locusts witnessed in Turkana County in 2020 [69]. Moreover, June recorded the highest decrease in vegetation greenness compared to the subsequent month of July, which showed a slight decrease in comparison to June. This change implies damage caused in croplands and pasturelands that are sources of livelihood to both pastoral and agro-pastoral communities. A DL swarm of approximately 150 million locusts per square kilometer can cause daily food hunger for about 2500 people with substantial pasture productivity losses [70]. Additionally, the decrease in vegetation greenness in June–July 2020 concurred with the observation of [69] who noted that the region was highly infested with DL hoppers. These hoppers caused damage to various vegetation types that included shrublands, grasslands, and dwarf grasslands with *Acacia reficiens* dominating the landscape and providing forage for most of the livestock [73]. We anticipated that the migration pattern and nature of feeding, together with the developmental stages of these hopper

bands caused the varying trend in NDVI levels as indicated in Figures 5–7. As a result, the loss in vegetation biomass and productivity as a function of NDVI could have reduced food production and severely impacted access to food and nutrition for agro-pastoral and pastoral livelihood-dependent zones that consistently indicated high DL observation densities across the three months. Hence, there is a need to develop early warning and decision support systems that can effectively monitor future DL invasions in order to protect the livelihoods of these already food-depressed regions.

#### 4.2. Predicted Desert Locust Invasion Risk Areas

The current and future geographical distribution for DLs was predicted using SSP2-4.5 (middle of the road) and SSP5-8.5 (maximum) climate projection narratives by applying the MaxEnt model principles that are widely accepted and used by several studies [20,22,24,25,61,74,75]. The relatively large DL presence records used in this study allowed the use of the LQPH feature class combination to predict the current and future suitable habitats for DL invasion. The results obtained in this study indicated a wider DL distribution range under current conditions compared to the future distribution that was predicted to be slightly reduced with climate change. Additionally, the results demonstrated that a very high suitability for DL invasion (0.6–1.0 probability) matched with the locations of invasion that were observed in the 2020 upsurge. However, the northern parts of the county remained relatively unsuitable for both current and future climate scenarios [14]. The 2030 climate projections predict a decrease in habitat suitability range, yet an environment that supports breeding and spread of the pest in the region [11].

The findings from other studies that have investigated the influence of climate change on global agricultural pests distribution concurred with our findings that rainfall and temperature have a significant influence on economically important pests [74–77]. Rainfall is one of the central climatic variables for DL invasion. Rainfall triggers vegetation onset and growth, which provides food and an attractive foraging habitat for the DLs. This is very important for DLs to develop and reproduce, particularly in their commonly dry habitats. In addition, rainfall improves soil moisture content, which is an important edaphic variable for the pest to lay its eggs [11]. Moreover, temperature determines the movement and migration rates of DLs over long distances and their feeding patterns and rate of egg development [2,76–78]. Moreover, temperature and rainfall cumulatively generate suitable conditions for DL reproduction and development. For instance, high rainfall and warmer temperatures are conducive conditions for DL breeding [78]. Our results indicated that the DL temperature tolerance range was within 20 °C–29.5 °C, and the geographical distribution suitability decreased sharply beyond 30 °C. Further, annual precipitation at an optimum range of approximately 175 mm–600 mm across the study area favored the propagation and successful breeding of the DLs [2]. The anticipated extreme weather events as a result of climate shifts would continue to influence the occurrence of this pest at varied scales in breeding and invasive sites across the affected regions. Therefore, our predictions in this study suggest that DL geographical coverage will decrease in the future with the SSP5–8.5 climate scenario indicating a decrease of about 6.80% in habitat coverage, which implies a significant spatial decrease of the suitable DL area in the future. Although this may seem a positive result, conditions that limit the DL propagation also limit the potential performance of crops, hence jeopardizing food and nutrition security. On the other hand, the future high to very-high suitability regions for DL occurrence will mostly be in areas of above-average rainfall that support significant vegetation growth, providing suitable conditions for DL breeding and propagation [79–81]. Consequently, these areas must be protected from both invasions as well as other adverse climatic food production constraints if they are to be sustainably food and nutrition secure. Moreover, in our vegetation dynamics analysis, most of the region showed considerable vegetation greenness reduction with high densities of DL observations. This points to an indicator of livelihood depression.



Furthermore, the predicted suitable DL habitats indicate a larger distribution range compared to the known DL occurrence and attack localities within the region. This implies that the coverage extends to remote areas that have not been surveyed to determine the presence of the pest due to the inaccessibility and remoteness of the sites, which is why this study utilized the robustness of Earth observation tools. This study thus provides an in-depth understanding of the status of vegetation during similar DL attacks and how such damage could affect livelihoods, especially in the marginalized regions across the entire DL occurrence and invasion range [14,76].

Overall, this study used multi-date S2 NDVI data to assess vegetation change as a function of DL damage. This approach is similar to what other earlier studies have used to investigate vegetation health [55,67,82,83]. Although in this study our modelling approach relied on climatic factors to inform the DL habitat distribution, future studies could also benefit from integrating other variables under current climatic conditions, such as wind speed and vegetation, for instance, NDVI and other vegetation dynamics. Despite the immense strengths provided by the S2, such as repetitive data coverage every five days and spatial resolution of 10 m, the use of higher resolution imagery such as WorldView-3 and RapidEye data could make it possible to discern finer and more subtle vegetation changes with less atmospheric contamination. Our findings can guide the establishment of priority zones for DL management, hence site-specific deployment of control options. Similarly, our study provides an assessment of vegetation productivity reduction due to DL invasion in the study area, which can be upscaled to other areas of potential DL invasion and upsurge in the central, western, and eastern regions in Africa. Furthermore, our study shows that DL invasion remains disastrous, and it can contribute to food insecurity and malnutrition in the invasion countries. Moreover, this study demonstrated the potential applicability of machine learning geospatial modelling techniques for assessing DL invasion and vegetation damage to a broader extent. This could cover both DL frontline and invasion countries in northern, central, western, and eastern Africa and beyond under current and projected climate shifts to contribute to the understanding of the global food and nutrition insecurity drivers. Notwithstanding, one of the limitations of our geospatial modelling approach is that we did not consider the inclusion of some relevant ecological variables to DL invasion, such as wind speed and direction and vegetation dynamics, in our models. In addition, invasion of DLs could depend on other geopolitical variables that might be difficult to simulate and predict.

## 5. Conclusions

This study demonstrated that the DL invasion has the potential to damage vegetation at the spatiotemporal scale. This severely impacts croplands and pasturelands, which in turn limits access to food in marginalized regions vulnerable to DL attack and invasion. Furthermore, future climate change will influence the geographical distribution of DLs, posing immense threats to new areas that are currently unsuitable for the development and survival of the DL species. The results demonstrated that the predicted distribution of suitable habitat for DLs is larger, with high suitability concentrating in areas of relatively higher rainfall. Therefore, continuous DL outbreak monitoring should be enhanced to provide timely and reliable information to help control operations and restrict their disturbance on marginalized communities' livelihoods in affected areas. So, this study provides potential DL invasion risk and vegetation damage in one of the key upsurge areas. Our approach could be extended to other locations within the migratory path of DLs. The study outputs could be integrated into the control and management plans that are currently used to inform surveillance and control operations of the pest for both current and potential future incidences. Concerned international institutions, local governments, and decision makers could use the information generated by this study as a baseline to inform early warning of the pest outbreak and estimate the impacts on food and nutrition security and access in various livelihood zones in the county.



**Author Contributions:** Conceptualization, E.M.A.-R., R.M. and E.K.; methodology, R.M., E.K., B.T.M. and E.M.A.-R.; formal analysis, R.M.; resources, S.O., H.E.Z.T., B.T.M. and E.M.A.-R.; data curation, R.M.; writing—original draft preparation, R.M.; writing—review and editing, R.M., E.M.A.-R., B.T.M., S.O. and H.E.Z.T.; supervision, E.M.A.-R., B.T.M., E.K. and S.O.; funding acquisition, E.M.A.-R. and H.E.Z.T. All authors have read and agreed to the published version of the manuscript.

**Funding:** The authors gratefully acknowledge the financial support for this research by the following organizations and agencies: the Swedish International Development Cooperation Agency (Sida); the Swiss Agency for Development and Cooperation (SDC); the Australian Centre for International Agricultural Research (ACIAR); the Federal Democratic Republic of Ethiopia; and the Government of the Republic of Kenya. The views expressed herein do not necessarily reflect the official opinion of the donors.

**Data Availability Statement:** The data that supports the findings of this study are available at <https://dmmg.icipe.org/dataportal/dataset/desert-locust-invasion-risk-and-vegetation-damage-in-key-upsurge-area>, accessed on 15 March 2023 while the codes used in the analysis are available at <https://github.com/icipe-official/desert-locust-invasion-risk-and-vegetation-damage-in-key-upsurge-area>, accessed on 15 March 2023.

**Conflicts of Interest:** The authors declare no conflict of interest.

## References

- Shrestha, S.; Thakur, G.; Gautam, J.; Acharya, N.; Pandey, M.; Shrestha, J. Desert locust and its management in Nepal: A review. *J. Agric. Nat. Resour.* **2021**, *4*, 1–28. [CrossRef]
- FAO; WMO. Weather and Desert Locusts. no. 1175. 2016. Available online: <https://www.preventionweb.net/publication/weather-and-desert-locust> (accessed on 29 January 2021).
- Chen, C.; Qian, J.; Chen, X.; Hu, Z.; Sun, J.; Wei, S.; Xu, K. Geographic distribution of desert locusts in Africa, Asia and Europe using multiple sources of remote-sensing data. *Remote Sens.* **2020**, *12*, 3593. [CrossRef]
- Waldner, F.; Ebbe, M.A.B.; Cressman, K.; Defourny, P. Operational monitoring of the desert locust habitat with earth observation: An assessment. *ISPRS Int. J. Geo-Inf.* **2015**, *4*, 2379–2400. [CrossRef]
- Wang, L.; Zhuo, W.; Pei, Z.; Tong, X.; Han, W.; Fang, S. Using long-term earth observation data to reveal the factors contributing to the early 2020 desert locust upsurge and the resulting vegetation loss. *Remote Sens.* **2021**, *13*, 680. [CrossRef]
- FAO. Desert Locust Bulletin: General Situation During January 2020 Forecast Until Mid-March 2020. 2020, vol. 52420, no. 496. Available online: <https://www.fao.org/ag/locusts/common/ecg/562/en/DL496e.pdf> (accessed on 15 March 2023).
- FAO. Desert Locust Component: Strengthening Desert Locust Management FAO's Response to the Desert Locust Problem. 2020. Available online: <https://www.fao.org/ag/locusts/common/ecg/1344/en/EMPRESbrochureE.pdf> (accessed on 15 March 2023).
- Brader, L.; Djibo, H.; Faya, F.G.; Ghaout, S.; Lazar, M.; Luzietoso, P.N.; Ould-Babab, M.A. Towards a more effective response to desert locusts and their impacts on food security, livelihood and poverty. In *Multilateral Evaluation of the 2003–05 Desert Locust Campaign*; Food and Agriculture Organisation: Rome, Italy, 2006; pp. 1–42.
- Showler, A. Desert locust control: The effectiveness of proactive interventions and the goal of outbreak prevention. *Am. Entomol.* **2019**, *65*, 180–191. [CrossRef]
- Salih, A.A.M.; Baraibar, M.; Mwangi, K.K.; Artan, G. Climate change and locust outbreak in East Africa. *Nat. Clim. Chang.* **2020**, *10*, 584–585. [CrossRef]
- Kimathi, E.; Tonnang, H.E.Z.; Subramanian, S.; Cressman, K.; Abdel-Rahman, E.M.; Tesfayohannes, M.; Niassy, S.; Torto, B.; Dubois, T.; Tanga, C.M.; et al. Prediction of breeding regions for the desert locust *Schistocerca gregaria* in East Africa. *Sci. Rep.* **2020**, *10*, 11937. [CrossRef]
- FAO. Impact of Desert Locust Infestation on Household Livelihoods and Food Security in Ethiopia. 2020; pp. 1–14. Available online: <https://reliefweb.int/report/ethiopia/impact-desert-locust-infestation-household-livelihoods-and-food-security-ethiopia#:~:text=According%20to%20the%20Assessment%20findings,wheat%20at%2036%20000%20hectares> (accessed on 27 May 2021).
- Kalakkal, J.; Singh, A. *Desert Locusts' Upsurges: A Harbinger of Emerging Climate Change Induced Crises*; The United Nations Environment Programme (UNEP): Nairobi, Kenya, 2021; Volume 22, pp. 1–10. Available online: <https://wedocs.unep.org/bitstream/handle/20.500.11822/34226/1/FB019.pdf> (accessed on 15 March 2023).
- FAO. Kenya Intensifies Desert Locust Control Measures in Turkana County. 2020. Available online: <https://www.fao.org/kenya/news/detail-events/en/c/1279309/#:~:text=Nairobi%2C> (accessed on 12 March 2021).
- Eltoum, M. Detection of change in vegetation cover caused by desert locust in Sudan. In *Proceedings of the SPIE Asia Pacific Remote Sensing*, Beijing, China, 13–16 October 2014.
- Cressman, K. Role of remote sensing in desert locust early warning. *J. Appl. Remote Sens.* **2013**, *7*, 075098. [CrossRef]
- Moustafa, O.R.M.; Cressman, K. Using the enhanced vegetation index for deriving risk maps of desert locust (*Schistocerca gregaria*, Forskal) breeding areas in Egypt. *J. Appl. Remote Sens.* **2015**, *8*, 084897. [CrossRef]

18. Latchininsky, A.V.; Sivanpillai, R. Locust habitat monitoring and risk assessment using remote sensing and GIS technologies. In *Integrated Management of Arthropod Pests and Insect Borne Diseases*; Springer: Dordrecht, The Netherlands, 2010. [\[CrossRef\]](#)
19. Zhu, Y.; Wei, W.; Li, H.; Wang, B.; Yang, X.; Liu, Y. Modelling the potential distribution and shifts of three varieties of *Stipa tianschanica* in the eastern Eurasian Steppe under multiple climate change scenarios. *Glob. Ecol. Conserv.* **2018**, *16*, e00501. [\[CrossRef\]](#)
20. Li, X.H.; Wang, J.H.; Xing, L.G.; Fu, Y.Y. MaxEnt modelling for predicting climate change effects on the potential planting area of tuber mustard in China. *J. Agric. Sci.* **2019**, *157*, 375–381. [\[CrossRef\]](#)
21. Li, Y.; Li, M.; Li, C.; Liu, Z. Optimized MaxEnt model predictions of climate change impacts on the suitable distribution of *Cunninghamia lanceolata* in China. *Forests* **2020**, *11*, 302. [\[CrossRef\]](#)
22. Liu, Y.; Shi, J. Predicting the potential global geographical distribution of two *Icerya* species under climate change. *Forests* **2020**, *11*, 684. [\[CrossRef\]](#)
23. Mudereri, B.T.; Kimathi, E.; Chitata, T.; Moshobane, M.C.; Abdel-Rahman, E.M. Landscape-scale biogeographic distribution analysis of the whitefly, *Bemisia tabaci* (Gennadius, 1889) in Kenya. *Int. J. Trop. Insect Sci.* **2021**, *41*, 1585–1599. [\[CrossRef\]](#)
24. Garah, K.; Bentouati, A. Using the MaxEnt model for assessing the impact of climate change on the Eurasian Aleppo pine distribution in Algeria. *Afr. J. Ecol.* **2019**, *57*, 500–511. [\[CrossRef\]](#)
25. Mtengwana, B.; Dube, T.; Mudereri, B.T.; Shoko, C. Modelling the geographic spread and proliferation of invasive alien plants (IAPs) into new ecosystems using multi-source data and multiple predictive models in the Heuningnes catchment, South Africa. *GIScience Remote Sens.* **2021**, *58*, 483–500. [\[CrossRef\]](#)
26. Hosni, E.M.; Nasser, M.G.; Al-Ashaal, S.A.; Rady, M.H.; Kenawy, M.A. Modelling current and future global distribution of *Chrysomya bezziana* under changing climate. *Sci. Rep.* **2020**, *10*, 4947. [\[CrossRef\]](#) [\[PubMed\]](#)
27. Naimi, B.; Araújo, M.B. Sdm: A reproducible and extensible R platform for species distribution modelling. *Ecography* **2016**, *39*, 368–375. [\[CrossRef\]](#)
28. Pearson, R.G.; Raxworthy, C.J.; Nakamura, M.; Townsend, P.A. Predicting species distributions from small numbers of occurrence records: A test case using cryptic geckos in Madagascar. *J. Biogeogr.* **2007**, *34*, 102–117. [\[CrossRef\]](#)
29. Phillips, S.J.; Anderson, R.P.; Schapire, R.E. Maximum entropy modelling of species geographic distributions. *Ecol. Modell.* **2006**, *190*, 231–259. [\[CrossRef\]](#)
30. Paudel, T.B.; Niassy, S.; Kimathi, E.; Abdel-Rahman, E.M.; Seidl-Adams, I.; Wamalwa, M.; Tonnang, H.E.Z.; Ekesi, S.; Hughes, D.P.; Rajotte, E.G.; et al. Potential distribution of fall armyworm in Africa and beyond, considering climate change and irrigation patterns. *Sci. Rep.* **2022**, *12*, 539. [\[CrossRef\]](#) [\[PubMed\]](#)
31. ESA. Sentinel-2 User Handbook, no. 1.2. European Space Agency. 2015. Available online: [https://sentinel.esa.int/documents/247904/685211/Sentinel-2\\_User\\_Handbook](https://sentinel.esa.int/documents/247904/685211/Sentinel-2_User_Handbook) (accessed on 21 June 2021).
32. KNBS. Kenya Population and Housing Census Volume 1: Population by County and Sub-County 2019; Volume I. Available online: <https://www.knbs.or.ke/?wpdmpromo=2019-kenya-population-and-housing-census-volume-i-population-by-county-and-sub-county> (accessed on 16 June 2021).
33. CIDP. Turkana County Integrated Development Plan (CIDP II) 2018–2022. Available online: <https://repository.kippra.or.ke/handle/123456789/2832> (accessed on 21 June 2021).
34. Opiyo, F.; Wasonga, O.; Nyangito, M.; Schilling, J.; Munang, R. Drought adaptation and coping strategies among the Turkana pastoralists of northern Kenya. *Int. J. Disaster Risk Sci.* **2015**, *6*, 295–309. [\[CrossRef\]](#)
35. Everlyne, E.; Roxvanta, O.; Jackline, K.; Samson, O.; Patrick, M.; Jesse, O. Plant species and their importance to housing in the Turkana community, Kenya. *J. Hortic. For.* **2020**, *12*, 101–108. [\[CrossRef\]](#)
36. Mbaluka, J.K.; Brown, F.H. Vegetation of the Koobi Fora region northeast of Lake Turkana, Marsabit county, northern Kenya. *J. East African Nat. Hist.* **2016**, *105*, 21–50. [\[CrossRef\]](#)
37. Kariuki, J.G.; Machua, J.; Luvanda, A.M.; Kigomo, J.N.; Muindi, F.K.; Macharia, E.W. Baseline Survey of Woodland Utilization and Degradation around Kakuma Refugee Camp (I). Kenya Forestry Research Institute (KEFRI), Nairobi, Kenya. Available online: <https://www.fornis.net/sites/default/files/documents/KEFRI%20JOFA%20Project%20Technical%20Report%20N01.pdf> (accessed on 21 June 2021).
38. Ngigi, W.T. Production of briquettes from *Prosopis juliflora* stem and anthill soil. *Int. J. Nov. Res. Phys. Chem. Math.* **2017**, *4*, 22–27.
39. Murayama, Y.; Ranagalage, M. Sentinel-2 data for land cover/use mapping: A review. *Remote Sens.* **2020**, *12*, 2291. [\[CrossRef\]](#)
40. Baillarin, S.; Lacherade, S.; Martimort, P.; Agency, E.S.; Spoto, F.; Agency, E.S. Sentinel-2 level 1 products and image processing performances. *Int. Arch. Photogramm. Remote Sens. Spatial Inf. Sci.* **2012**, XXXIX-B1, 197–202. [\[CrossRef\]](#)
41. Eyring, V.; Bony, S.; Meehl, G.A.; Ronald, S.; Oceanic, N. Overview of the coupled model intercomparison project phase 6 (CMIP6) experimental design and organisation. *Geosci. Model Dev. Discuss.* **2015**, *8*, 10539–10583. [\[CrossRef\]](#)
42. R Core Team. R: A Language and Environment for Statistical Computing. 2021, 2. Available online: <https://www.r-project.org/> (accessed on 21 June 2021).
43. Wickham, H. Ggplot2: Elegant Graphics for Data Analysis 2016, 35. Available online: <http://had.co.nz/ggplot2/book> (accessed on 16 October 2021).
44. Cressman, K. Desert locust guidelines. 2. Survey, Food Agric. Organ. United Nations, p. viii + 56pp. 2001. Available online: [http://www.fao.org/ag/LOCUSTS/common/ecg/347\\_en\\_DLG2e.pdf](http://www.fao.org/ag/LOCUSTS/common/ecg/347_en_DLG2e.pdf) (accessed on 29 January 2021).

45. Fick, S.E.; Hijmans, R.J. WorldClim 2: New 1-km spatial resolution climate surfaces for global land areas. *Int. J. Climatol.* **2017**, *37*, 4302–4315. [CrossRef]
46. Tatebe, H.; Ogura, T.; Nitta, T.; Komuro, Y.; Ogochi, K.; Takemura, T.; Sudo, K.; Sekiguchi, M.; Abe, M.; Saito, F.; et al. Description and basic evaluation of simulated mean state, internal variability, and climate sensitivity in MIROC6. *Geosci. Model Dev.* **2018**, *12*, 2727–2765. [CrossRef]
47. Hijmans, R.J.; Etten, J.V.; Sumner, M.; Cheng, J.; Baston, D.; Bevan, A.; Bivand, R.; Busetto, L.; Canty, M.; Fasoli, B.; et al. Raster: Geographic Data Analysis and Modelling. R package version 3.3–7. 2020. Available online: <https://cran.r-project.org/package=raster> (accessed on 21 June 2021).
48. Roy, D.P.; Li, J.; Zhang, H.K.; Yan, L. Best practices for the reprojection and resampling of sentinel-2 multi spectral instrument level 1c data. *Remote Sens. Lett.* **2016**, *7*, 1023–1032. [CrossRef]
49. Leroy, B.; Meynard, C.N.; Bellard, C.; Courchamp, F. Virtualspecies, an R package to generate virtual species distributions. *Ecography* **2015**, *39*, 599–607. [CrossRef]
50. IPCC. Assessment Report 6 Climate Change 2021: The Physical Science Basis. 2021. Available online: <https://www.ipcc.ch/report/ar6/wg1/> (accessed on 15 November 2021).
51. Meinshausen, M.; Nicholls, Z.; Lewis, J.; Gidden, M.; Vogel, E.; Freund, M.; Beyerle, U.; Gessner, C.; Nauels, A.; Bauer, N.; et al. The SSP greenhouse gas concentrations and their extensions to 2500. *Geosci. Model Dev. Discuss.* **2019**, *13*, 3571–3605. [CrossRef]
52. Ali, S.M.; Jassem, D.R. Monitoring vegetation areas by using remote sensing techniques. *Int. J. Comp. Info. Tech.* **2015**, *3*, 1–9. [CrossRef]
53. Neigh, C.S.R.; Tucker, C.J.; Townshend, J.R.G. North American vegetation dynamics observed with multi-resolution satellite data. *Remote Sens. Environ.* **2008**, *112*, 1749–1772. [CrossRef]
54. Pettorelli, N.; Ryan, S.; Mueller, T.; Bunnefeld, N. The normalized difference vegetation index (NDVI): Unforeseen successes in animal ecology. *Clim. Res.* **2011**, *46*, 15–27. [CrossRef]
55. Schmid, J.N. Using Google Earth Engine for Landsat NDVI Time Series Analysis to Indicate the Present Status of Forest Stands. Bachelor's Thesis, Georg-August-Universität Göttingen, Göttingen, Germany, October 2017. [CrossRef]
56. Mutanga, O.; Kumar, L. Google Earth Engine applications. *Remote Sens.* **2019**, *11*, 591. [CrossRef]
57. Sivarajah, M. An Introduction to Google Earth Engine javascript API. 2019, 416–424. Available online: <https://earthengine.google.com/%0Ahttps://sovzond.ru/press-center/news/corporate/6095/> (accessed on 28 June 2021).
58. Bey, A.; Jetimane, J.; Lisboa, S.N.; Ribeiro, N.; Siteo, A.; Meyfroidt, P. Mapping smallholder and large-scale cropland dynamics with a flexible classification system and pixel-based composites in an emerging frontier of Mozambique. *Remote Sens. Environ.* **2020**, *239*, 111611. [CrossRef]
59. Hashim, H.; Abd-Latif, Z.; Adnan, N.A. Urban vegetation classification with NDVI threshold value method with very high resolution (VHR) Pleiades imagery. *Int. Arch. Photogramm. Remote Sens. Spat. Inf. Sci.* **2019**, *42*, 237–240. [CrossRef]
60. Baloch, M.N.; Fan, J.; Haseeb, M.; Zhang, R. Mapping potential distribution of *Spodoptera frugiperda* (Lepidoptera: Noctuidae) in Central Asia. *Insects* **2020**, *11*, 172. [CrossRef]
61. Elith, J.; Phillips, S.J.; Hastie, T.; Dudík, M.; Chee, Y.E.; Yates, C.J. A statistical explanation of MaxEnt for ecologists. *Divers. Distrib.* **2011**, *17*, 43–57. [CrossRef]
62. Phillips, S.J. A Brief Tutorial on MaxEnt. *AT&T Res.* **2018**, *190*, 231–259.
63. Muscarella, R.; Galante, P.J.; Soley-guardia, M.; Boria, R.A.; Kass, J.M.; Anderson, R.P. ENMeval: An R package for conducting spatially independent evaluations and estimating optimal model complexity for maxent ecological niche models. *Methods Ecol. Evol.* **2014**, *5*, 1198–1205. [CrossRef]
64. Arthur, F.H.; Iii, W.R.M.; Morey, A.C. Modelling the potential range expansion of larger grain borer, *Prostephanus truncatus* (Coleoptera: Bostrichidae). *Sci. Rep.* **2018**, *9*, 6862. [CrossRef] [PubMed]
65. Qin, A.; Liu, B.; Guo, Q.; Bussmann, R.W.; Ma, F.; Jian, Z.; Xu, G.; Pei, S. MaxEnt modelling for predicting impacts of climate change on the potential distribution of *Thuja sutchuenensis* Franch., an extremely endangered conifer from southwestern China. *Glob. Ecol. Conserv.* **2017**, *10*, 139–146. [CrossRef]
66. Merow, C.; Smith, M.J.; Silander, J.A. A practical guide to MaxEnt for modelling species' distributions: What it does, and why inputs and settings matter. *Ecography* **2013**, *36*, 1058–1069. [CrossRef]
67. Adan, M.; Abdel-Rahman, E.M.; Gachoki, S.; Muriithi, B.W.; Lattorff, H.M.G.; Kerubo, V.; Landmann, T.; Mohamed, S.A.; Tonnang, H.E.Z.; Dubois, T. Use of earth observation satellite data to guide the implementation of integrated pest and pollinator management (IPPM) technologies in an avocado production system. *Remote Sens. Appl. Soc. Environ.* **2021**, *23*, 100566. [CrossRef]
68. Roberts, D.; Mueller, N.; McIntyre, A. High-dimensional pixel composites from earth observation time series. *IEEE Trans. Geosci. Remote Sens.* **2017**, *55*, 6254–6264. [CrossRef]
69. NDMA. *Turkana County Drought Early Warning Bulletin for July 2020*; National Drought Management Authority: Nairobi, Kenya, 2020; pp. 1–14.
70. WMO. Heavy rains contribute to desert locust crisis in East Africa. 2020. Available online: <https://public.wmo.int/en/media/news/heavy-rains-contribute-desert-locust-crisis-east-africa> (accessed on 13 July 2021).
71. Zhang, W.; Brandt, M.; Tong, X.; Tian, Q.; Fensholt, R. Impacts of the seasonal distribution of rainfall on vegetation productivity across the Sahel. *Biogeosciences* **2018**, *15*, 319–330. [CrossRef]

72. Mohamed, N.; Bannari, A. The relationship between vegetation and rainfall in central Sudan. *Int. J. Remote Sens. Appl.* **2016**, *6*, 30. [CrossRef]
73. Turkana County Government. Turkana County climate Change Policy 2020 Draft 1. 2020. Available online: <https://www.turkana.go.ke/wp-content/uploads/2020/09/Book.pdf> (accessed on 13 July 2021).
74. Yang, X.Q.; Kushwaha, S.P.S.; Saran, S.; Xu, J.; Roy, P.S. MaxEnt modelling for predicting the potential distribution of medicinal plant, *Justicia adhatoda* L. in Lesser Himalayan foothills. *Ecol. Eng.* **2013**, *51*, 83–87. [CrossRef]
75. Çoban, H.O.; Özücü, Ö.K.; Arslan, E.S. MaxEnt modelling for predicting the current and future potential geographical distribution of *Quercus libani* Olivier. *Sustainability* **2020**, *12*, 2671. [CrossRef]
76. Nayak, S.B.; Rao, K.S.; Ramalakshmi, V. Impact of climate change on insect pests and their natural enemies *Sudhanshu*. *Int. J. Ecol. Environ. Sci.* **2020**, *2*, 579–584.
77. Skendžić, S.; Zovko, M.; Živković, I.P.; Lešić, V.; Lemić, D. The impact of climate change on agricultural insect pests. *Insects* **2021**, *12*, 440. [CrossRef]
78. Symmons, P.M.; Cressman, K. *Desert Locust Guidelines, Biology and behaviour*, 2nd ed.; Food and Agriculture Organization, United Nations: Rome, Italy, 2001; p. 42.
79. Borzée, A.; Andersen, D.; Groffen, J.; Kim, H.T.; Bae, Y.; Jang, Y. Climate change-based models predict range shifts in the distribution of the only Asian plethodontid salamander: *Karsenia koreana*. *Sci. Rep.* **2019**, *9*, 11838. [CrossRef]
80. Olang, M.O. *Vegetation Cover Assessment in Turkana District, Kenya*; International Institute for Land Reclamation and Improvement: Wageningen, The Netherlands, 1983; pp. 183–193.
81. Garrido, R.; Bacigalupo, A.; Peña-Gómez, F.; Bustamante, R.O.; Cattán, P.E.; Gorla, D.E.; Botto-Mahan, C. Potential impact of climate change on the geographical distribution of two wild vectors of Chagas disease in Chile: *Mepraia spinolai* and *Mepraia gajardoi*. *Parasites Vectors* **2019**, *12*, 478. [CrossRef] [PubMed]
82. Gandhi, G.M.; Parthiban, S.; Thummalu, N.; Christy, A. Ndv: Vegetation change detection using remote sensing and GIS—A case study of Vellore district. *Procedia Comput. Sci.* **2015**, *57*, 1199–1210. [CrossRef]
83. Oikonomopoulos, E. NDVI Time Series Analysis for Desert Locust Outbreak Detection and Quantification Analysis of Its Impact on Vegetation Productivity of Sahel. Master's Thesis, Lund University, Lund, Sweden, 2020.

**Disclaimer/Publisher's Note:** The statements, opinions and data contained in all publications are solely those of the individual author(s) and contributor(s) and not of MDPI and/or the editor(s). MDPI and/or the editor(s) disclaim responsibility for any injury to people or property resulting from any ideas, methods, instructions or products referred to in the content.